Seamless Mobile Indoor Navigation With VLP-PDR

Aitor Alcázar-Fernández, Álvaro De-La-Llana-Calvo, José Luis Lázaro-Galilea, *Member, IEEE*, Antoni Pérez-Navarro, *Member, IEEE*, Rubén Gil-Vera, and Alfredo Gardel-Vicente

***Abstract*—This study unveils a mobile app-based indoor positioning system (IPS) tailored for seamless museum navigation. Leveraging smartphone inertial measurement unit (IMU) sensors, it incorporates a pedestrian dead reckoning (PDR) algorithm and a visible light positioning (VLP) beacon-based angle of arrival (AoA) algorithm for precise user positioning relative to smart light sources. In standalone mode, the VLP AoA-based algorithm demonstrates reliability with a mean error of 10.64 cm, while the PDR algorithm, operating independently, exhibits mean error of 3 m influenced by environmental factors. Integration of both algorithms proves crucial in mitigating cumulative errors. By updating PDR deviations with the precision provided by the VLP AoA-based solution, the entire system minimizes its mean error to 0.85 m. The user-friendly interface not only enriches visitor experiences with contextual information but also enables intuitive navigation without continuous internet connectivity. This innovative solution caters to the critical demand for precise indoor navigation, particularly in museum environments, fostering increased user acceptance and utilization.**

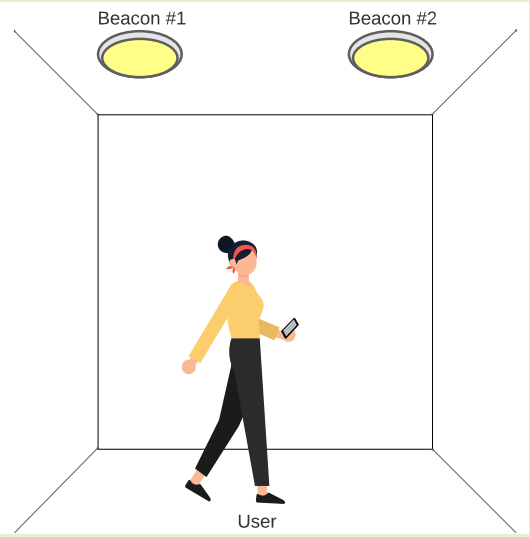

***Index Terms*— Android, angle of arrival (AoA), inertial measurement unit (IMU), smartphone, visible light positioning (VLP).**

I. Introduction

IN THE digital age, technological advancements have had a profound impact on various aspects of our daily lives. These innovations have revolutionized the way we interact with the world, leading to improved efficiency in both work and daily activities [1]. Museums and exhibition spaces have also embraced these technological advancements, with a growing interest in implementing indoor positioning technologies in recent years [2], [3].

Indoor positioning systems (IPSs) enable the localization of people and objects within enclosed spaces using diverse technologies. These systems find applications in indoor navigation, security, and inventory management, among others [4], [5], [6], [7].

Infrared technology relies on the emission and detection of infrared signals to measure the distance between a transmitter and a receiver. However, this technology has limited range and can be susceptible to signal blockage by objects. A system proposed in [8] utilizes four infrared LEDs and a quadrant angular diversity aperture receiver (QADA), leveraging coding techniques to determine the receiver's position based on the incidence points of the infrared transmitters. The system exploits the geometrical characteristics of the setup, including the polar angle and its relation to the receiver position, the angle of incidence, and the aperture height. Another example can be found in [9], where infrared beacons are employed for dynamic and static measurements in a metal shelving environment, simulating real retail and warehouse settings.

Ultrasonic sensor-based systems employ time-of-flight measurements of ultrasonic signals to determine the distance

Manuscript received 4 February 2024; accepted 17 February 2024. Date of publication 27 February 2024; date of current version 2 April 2024. This work was supported in part by the University of Alcalá (UAH) through the Project "Desarrollo de focos luminosos para aplicaciones conjuntas de emergencia y localización (LUZEMER)" under Grant PIUAH23/IA-038 and in part by the REd de Posicionamiento y Navegación en INteriores y exteriores restringidos y sus aplicaciones (REPNIN++) funded by MCIN/AEI/10.13039/501100011033 under Grant RED2022-134355-T. The associate editor coordinating the review of this article and approving it for publication was Dr. Tai Fei. *(Corresponding author: Aitor Alcázar-Fernández.)*

Aitor Alcázar-Fernández, Álvaro De-La-Llana-Calvo, José Luis Lázaro-Galilea, Rubén Gil-Vera, and Alfredo Gardel-Vicente are with the Department of Electronics, University of Alcalá, 28805 Alcalá de Henares, Spain (e-mail: aitor.alcazar@uah.es; alvaro.llana@uah.es; josel.lazaro@uah.es).

Antoni Pérez-Navarro is with the Faculty of Computer Sciences, Multimedia and Telecommunication, Universitat Oberta de Catalunya, 08860 Barcelona, Spain.

Digital Object Identifier 10.1109/JSEN.2024.3368169

© 2024 The Authors. This work is licensed under a Creative Commons Attribution-NonCommercial-NoDerivatives 4.0 License.
For more information, see https://creativecommons.org/licenses/by-nc-nd/4.0/

between the transmitter and receiver. While these systems offer accuracy, they can be influenced by interference from other electronic devices and may encounter accuracy issues in noisy environments.

Recent studies have explored these technologies further, including the work described in [10] and [11]. The former presents a 3-D ultrasonic local positioning system that utilizes three independent systems to cover the entire workspace, integrating the information with Kalman filters. The latter introduces a positioning system that employs ultrasonic measurements and inertial sensors to calculate the position of a device. It also utilizes ultrasonic local positioning systems to correct cumulative errors.

Conversely, visible light-based systems offer accurate localization of users and their environment, making them a promising option for indoor guidance systems. Visible light positioning (VLP) systems have emerged as a promising alternative for indoor positioning solutions. A comprehensive investigation of visible light LED-based positioning technology for indoor object localization is presented in [12]. This study classifies and elaborates on relevant positioning algorithms and designs, comparing the performance of LED-based IPSs. Additionally, this article discusses advancements, challenges, and future research directions in VLP positioning systems. Orientation estimation results from a local positioning system based on PSD sensors and visible light emitted by visible light trails are presented in [13].

Inertial measurement units (IMUs) enable the implementation of navigation by estimation or inertial navigation principles. This approach involves estimating the position of a target using data sensed by the IMU. When applied to user navigation, it is known as human inertial navigation or pedestrian dead reckoning (PDR).

While numerous works are based on PDR, as mentioned in [14] and [15], most cases require the use of an external IMU. However, this work focuses on exclusive use of a smartphone. A general equation for implementing a pedestrian inertial navigation algorithm, regardless of how the device is held, is presented in [16]. On the other hand, Li and Ning [17] implement an algorithm dependent on the user's position, benefiting from device calibration using georeferenced maps. An interesting approach to improve the accuracy of PDR is studied in [18], where a particle filter is used.

This study focuses on determining the user's position by detecting a single smart light source through a mobile device's camera sensor. To achieve this, we profit the camera rolling shutter working mode and the pinhole model, implementing a VLP angle of arrival (AoA)-based algorithm for the detection and identification of various smart lights. The goal is to obtain the user's position when recognized by the device, applying a geometrical correction to refine the accuracy. However, in this environment, user positioning is contingent upon detecting a luminary. To overcome this limitation, we employ a PDR algorithm that utilizes the device's inertial sensors to estimate the user's position when a light source is undetected. The integration of both algorithms ensures a seamless IPS solution. In summary, this article encompasses the design, implementation, and evaluation of a mobile application incorporating these indoor positioning technologies. This application not only determines the user's position but also provides contextual information about the environment, facilitating seamless navigation within indoor spaces.

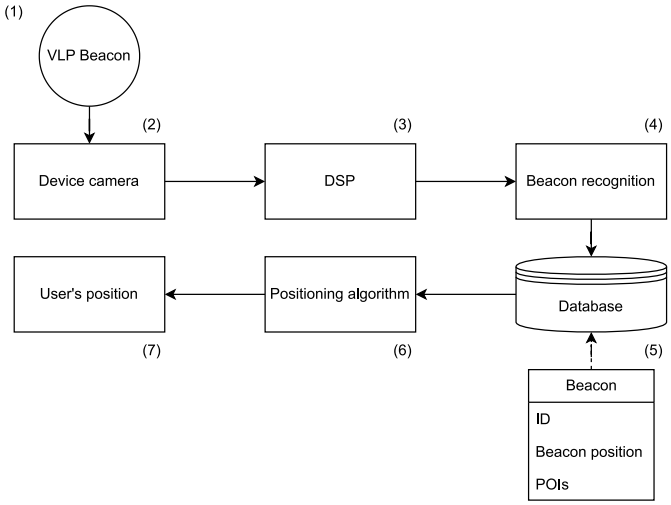

Fig. 1. Flow diagram of the mobile application.

During this study, Section II is aimed to describe the workflow of the application. Then, the two algorithms that define the solution are exposed as an in-depth analysis of the proposal in Sections III and IV. Then, the results present the standalone capabilities of both VLP AoA-based and PDR solutions, the integration of the algorithms, and the user interface (covered in Section V). Finally, the outcomes of the research as well as the next steps are exposed in the conclusion (Section VI).

II. Application for Indoor Positioning

The system proposed utilizes strategically placed intelligent light fixtures within the space to emit encoded signals that are detected by users' mobile applications.

Users can download the mobile application on their devices and use it as a receiver to capture the encoded signals from the luminaries. VLP technology enables the mobile application to determine the user's real-time location using visible light as the positioning source. By receiving the encoded signals from the luminaries, the application can accurately determine the user's precise location.

To further enhance positioning accuracy, the system incorporates PDR, which utilizes the motion sensors of the user's mobile device to calculate the distance and direction of the user's movement within the museum, thereby providing more precise location estimation.

Fig. 1 illustrates the flow diagram that governs the logic of the mobile application.

1) The VLP beacon is the first component in the process. This device emits a coded signal through visible light modulation, with the information being an identifier of the intelligent light fixture itself (which will be the same as the ID field in the database). The signal is used to identify the light fixture's position in space.
2) The next component is the mobile device camera sensor. This component captures the coded signal emitted by

the VLP beacon. The mobile device's camera is used to obtain an image of the light signal using the rolling shutter technique.

3) The digital signal processor or DSP is responsible for decoding the signal obtained by the mobile device's camera. Decoding is the process of extracting the ID from the encoded light signal.
4) Once the signal has been decoded, a beacon identification is performed by comparing the parameters of the coded signal with those stored in the database. If the parameters match, the beacon is identified.
5) The database contains objects of type beacon with parameters such as ID, position, and point of interest (POI). The position of the beacon is used to calculate the user's position.
6) The positioning algorithm utilizes the position of the identified beacon, the inclinations of the mobile device, and its physical characteristics to calculate the user's position.
7) Finally, the calculated position information from the positioning algorithm is used to update the user's position. This information can be displayed in the graphical interface of the mobile device, such as the interactive map. Additionally, contextual information based on the POIs can be displayed, with accessible options and multiple language choices.

III. In-Depth: VLP AoA-Based Algorithm for Position Correction

This section delves into an AoA-based algorithm aligned with the pinhole principle, exploring the key components and concepts that contribute to its effectiveness on implementing a VLP solution. Sections III-A and III-B examine various aspects of this algorithm to gain a comprehensive understanding of its inner workings.

Typically, users hold the mobile device in their hands, facing upward and aligned with its direction. This specific orientation of the device is referred to as the natural position, as illustrated in Fig. 2(a). When the user is positioned directly beneath the initial position of the luminary shadow in the natural position, the point calculated according to the AoA algorithm is $(0, 0)$. Nevertheless, this natural position might be changed with slight inclinations of the device. As shown in Fig. 2(b), this inclinations change the relative position of the emitter while is detected by the receiver, producing a positioning error. Furthermore, when the user moves within the coverage area of the luminary, this relative position introduces errors added to the produced by the inclinations of the device.

A. Pinhole Model for AoA Calculation

Fig. 3 shows the pinhole model diagram for the mobile device, which is discrete image sensors with $n \times m$ pixels. (X_w, Y_w, Z_w) are the coordinates of the world reference system, (X_R, Y_R, Z_R) are the coordinates in the mobile device reference system, and (X_r, Y_r, Z_r) are the coordinates of the camera referred to the world reference system. The impact point on the smartphone is represented as (x_i, y_i), where the

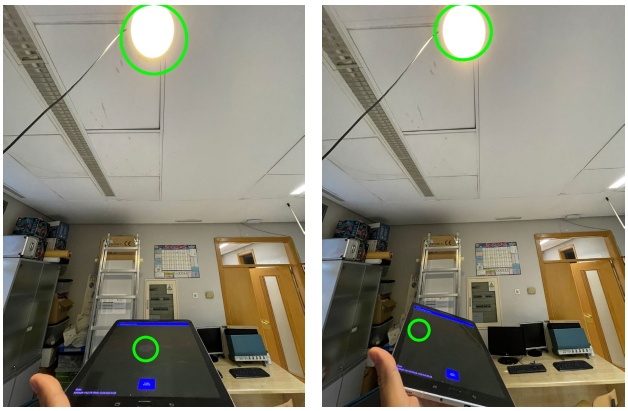

(a) (b)

Fig. 2. (a) Natural position. (b) Device inclined.

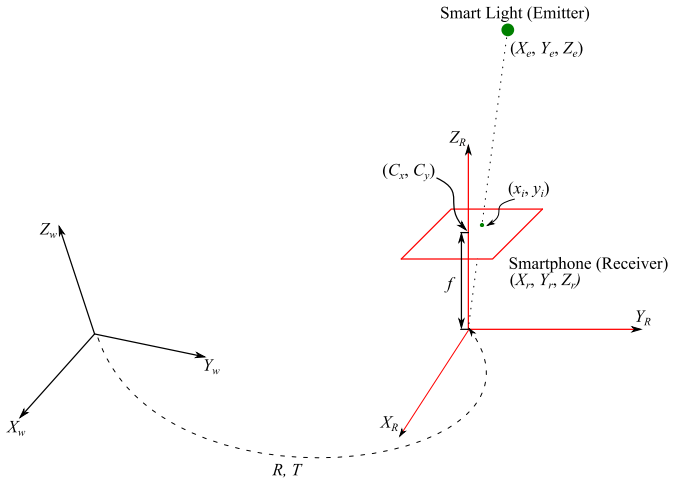

Fig. 3. Pinhole model diagram with the smartphone.

focal distance of the optics (device's camera) is represented as f, and the optic center is represented as (C_x, C_y). The rotation and translation matrices that relate the two reference systems, the world reference and the device reference, are denoted as R and T, respectively.

Furthermore, the relationship between the 3-D coordinates of the emitter (X_e, Y_e, Z_e) and the 2-D coordinates of the point of impact on the mobile device (x_i, y_i) is defined as follows:

$$\begin{pmatrix} sx_i \\ sy_i \\ s \end{pmatrix} = \underbrace{\begin{pmatrix} f & 0 & C_x \\ 0 & f & C_y \\ 0 & 0 & 1 \end{pmatrix}}_{\mathbf{A}} \underbrace{\begin{pmatrix} r_{11} & r_{12} & r_{13} \\ r_{21} & r_{22} & r_{23} \\ r_{31} & r_{32} & r_{33} \end{pmatrix}}_{\mathbf{R}} \begin{pmatrix} X_e - X_r \\ Y_e - Y_r \\ Z_e - Z_r \end{pmatrix} \quad (1)$$

where s is the projection scale factor, f is the device's sensor focal length, (C_x, C_y) are the coordinates of its optical center, $\mathbf{A}$ is the 3×3 device parameters' matrix, and $\mathbf{R}$ is the 3×3 rotation matrix (device orientation).

The values of the matrices $\mathbf{A}$ and $\mathbf{R}$ and the height of the smart light (emitter) Z_e and of the device Z_r are assumed to be known. Therefore, the receiver position (X_r, Y_r, Z_r) is obtained as

$$\begin{pmatrix} X_r \\ Y_r \\ Z_r \end{pmatrix} = -\mathbf{R}^{-1}\mathbf{A}^{-1} \begin{pmatrix} x_i \\ y_i \\ 1 \end{pmatrix} s + \begin{pmatrix} X_e \\ Y_e \\ Z_e \end{pmatrix}. \quad (2)$$

If the vector $\mathbf{q}$ is defined as

$$\mathbf{q} = \begin{pmatrix} q_1 \\ q_2 \\ q_3 \end{pmatrix} = -\mathbf{R}^{-1}\mathbf{A}^{-1} \begin{pmatrix} x_i \\ y_i \\ 1 \end{pmatrix} \tag{3}$$

and the value of the scaling factor s

$$s = \frac{Z_r - Z_e}{q_3} \tag{4}$$

receiver position is obtained as

$$\begin{pmatrix} X_r \\ Y_r \\ Z_r \end{pmatrix} = \mathbf{q}s + \begin{pmatrix} X_e \\ Y_e \\ Z_e \end{pmatrix}. \tag{5}$$

In conclusion, knowing all the values of (5), the position of the user can be obtained despite the disturbances in the orientation angle of the device. That is, the position of the device is corrected in such a way that it does not affect the position obtained from the user.

B. Parameters of the Device

As shown in (1), the equations are directly related with the mobile device parameters, such as the intrinsic matrix $\mathbf{A}$ and the extrinsic matrix $\mathbf{R}$.

1) Intrinsic Matrix A: The coordinates of the optical center of the camera are obtained through the geometry of the device, which relate the size of the pixel $d \times d$, with the rows w and columns h of the images it captures the sensor. Assume that the optical center coincides with the geometric center of the sensor, as will be assumed here (acknowledging a slight error). Thus,

$$C_x = d\frac{w}{2}, \quad C_y = d\frac{h}{2}. \tag{6}$$

Knowing the values of the coordinates of the optical center of the device (C_x and C_y) and the focal length (f), the matrix $\mathbf{A}$ can be written as

$$\mathbf{A} = \begin{pmatrix} f & 0 & d\frac{w}{2} \\ 0 & f & d\frac{h}{2} \\ 0 & 0 & 1 \end{pmatrix}. \tag{7}$$

2) Extrinsic Matrix R: The rotation matrix or extrinsic matrix $\mathbf{R}$ is obtained by rotating the Euler angles, which are defined, thanks to the device sensors, as: $\mathbf{R}_X(\phi)$ for the roll, $\mathbf{R}_Y(\theta)$ for pitch, and $\mathbf{R}_Z(\psi)$ for azimuth

$$\mathbf{R}_X(\phi) = \begin{pmatrix} 1 & 0 & 0 \\ 0 & \cos\phi & -\sin\phi \\ 0 & \sin\phi & \cos\phi \end{pmatrix} \tag{8}$$

$$\mathbf{R}_Y(\theta) = \begin{pmatrix} \cos\theta & 0 & \sin\theta \\ 0 & 1 & 0 \\ -\sin\theta & 0 & \cos\theta \end{pmatrix} \tag{9}$$

$$\mathbf{R}_Z(\psi) = \begin{pmatrix} \cos\psi & -\sin\psi & 0 \\ \sin\psi & \cos\psi & 0 \\ 0 & 0 & 1 \end{pmatrix}. \tag{10}$$

The rotation matrix $\mathbf{R}$ is obtained by multiplying the rotations of the Euler angles around the axes [obtained in (8)–(10)]

$$\mathbf{R} = \mathbf{R}_Z(\psi)\,\mathbf{R}_Y(\theta)\,\mathbf{R}_X(\phi). \tag{11}$$

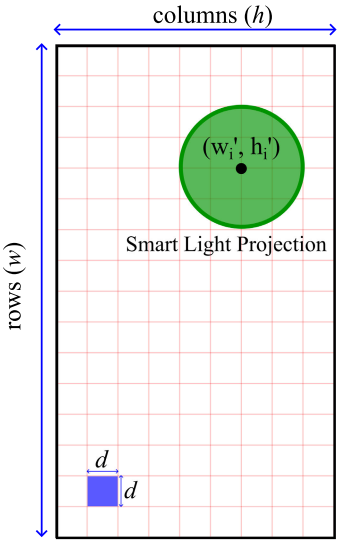

Fig. 4. Impact point projection of the smart light in the smartphone.

3) Impact Point: The impact point (x_i, y_i) is determined in the application, thanks to a circle detection algorithm. This algorithm recognizes circular shapes and obtains the position of the center of the smart light in the captured image and its radius. These values are related to the device parameters so that the optical center coincides with the center of impact.

Fig. 4 depicts the parameters related with the mobile device's image after a smart light is recognized. The impact point in rows and columns (w_i', h_i') is the one obtained by the sensor, the red grid illustrates the pixels matrix of the device, the pixel size is $d \times d$, the number of rows is w, and the number of columns is h. On the other hand, the smart light projection detected is illustrated on the screen in green.

To obtain the impact point (x_i, y_i), measured in mm, the following equation is used. This equation relates the information obtained through the camera sensor by using the values of the pixel size $d \times d$, the number of rows w and the number of columns h, and the impact point in rows and columns (w_i', h_i'). The outcome of the equation is to obtain the impact point in mm and use it in (1), as illustrated in Fig. 3

$$\begin{cases} x_i = d \cdot \left(w - w_i'\right) \\ y_i = d \cdot \left(h - h_i'\right). \end{cases} \tag{12}$$

4) Receiver Height and Emitter Position: The height of the receiver Z_r corresponds to the distance between the center of the device and the ground. In order to generalize this value, this value is selected as a constant for the experiments.

The position of the emitter (X_e, Y_e, Z_e) is obtained after the light source has been identified, by using the content parsed from the database (as shown in Fig. 1). As in the deployment of the intelligent lighting network, the bulbs are arranged in known positions, when the application determines if one bulb or another has been detected, its position is also known.

C. Modeling the Correction Algorithm on Android Platforms

The application utilizes Kotlin programming language to implement corrections in positioning measurements based on

AoA and the pinhole model. The device parameters are defined, including the number of columns and rows of the photograph, pixel size, and focal length. These parameters are used to construct the intrinsic matrix **A**.

To obtain the Euler angles, two methods provided by the Android API, namely, getRotationMatrix and getOrientation, are utilized. These methods make use of the accelerometer and magnetometer sensors to calculate the angles. The output of getOrientation is an array of three elements representing the azimuth, pitch, and roll angles.

Next, the rotation matrix **R** is derived using the obtained Euler angles. The rotation matrix is calculated based on azimuth, pitch, and roll rotations using trigonometric functions.

The impact point on the device is encoded as a vector, and the receiver position is defined as another vector. By computing the inverse of R and A matrices and multiplying them with the impact vector, a new vector q is obtained. The scale factor s is calculated based on the difference in Z-coordinates between the receiver and emitter positions. Finally, the receiver position is computed using the pinhole model for a single emitter.

IV. In-Depth: PDR-Based Algorithm for Position Estimation

In this work, improvements are proposed in obtaining the user's position, giving a solution to the losses in the location due to the absence of luminaries captured when the user moves. In this case, the device's inertial sensors (IMU) are used to estimate the user's position by analyzing their gait (PDR).

Following the study of numerous authors [14], [15], [16], a general equation of the PDR algorithm is formulated in order to provide an estimate in the changes of the user's position. In this case, the following equation can be written:

$$\begin{cases} X_k = X_{k-1} + L_{k-1,k} \cdot \sin\left(\psi_{k-1,k}\right) \\ Y_k = Y_{k-1} + L_{k-1,k} \cdot \cos\left(\psi_{k-1,k}\right) \end{cases} \tag{13}$$

where X and Y are the easting and northing coordinates (referring to georeferenced systems), L is the step length, ψ is the direction of the user during a step, and k denotes the index of the user step.

Sections IV-A–IV-C define the way that each parameter of (13) is calculated through the application.

A. Step Detection

The parameter k of the general equation (13) refers to the event produced in each user step. That is, each time the user takes a step, there is a new sample in the equation.

The device's inertial sensors are used to capture the user's movements. Specifically, the accelerometer is used to analyze the movement of the device when the user is walking and looking at the device at the same time (desired situation in the project application). In this condition, the smartphone is held in the natural position; therefore, the device will go up and down (oscillatory movement) as it moves forward. This produces a sinusoidal signal on the z-axis of the device, and the maximums represent each step k.

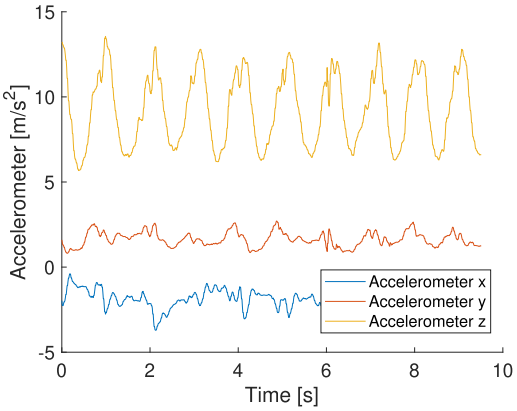

Fig. 5. Signal obtained from the accelerometer in the coordinate axes.

In Fig. 5, the signals obtained from the accelerometer are shown with respect to the three coordinate axes when a user walks under the described conditions. The value of the signal on the z-axis has its mean value around the value of the acceleration due to gravity on the surface of the Earth $g = 9.8$ m/s^2.

If the module of the three signals is obtained, the total variations produced by the device in the same signal can be represented. To extract the maximum value of the signal, a threshold value is set from which it is decided whether a step has occurred or not. It should be noted that, as documented in various implementations of PDR algorithms such as [15] and [16], this threshold directly depends on the way the user walks and different positions of the device. In this sense, a threshold of 11.2 m/s^2 has been established as a general value for most users based on the results obtained in these works.

On the other hand, it can be seen that due to the existing noise produced by the sensitivity of the sensor, there might be false positives in the detection of the maximums. To mitigate this effect, it is decided to perform a low-pass filter with infinite impulse response that guarantees an approximation to the desired sinusoidal signal. The used equation for such filter is presented in the following equation:

$$y\,[i] = y\,[i-1] + \alpha\,(x\,[i] - y\,[i-1]) \tag{14}$$

where i is the current instant, $i-1$ is the previous instant, y is the output signal, x is the input signal, and α is the smoothing factor.

The value of the smoothing factor is obtained by the relationship between the time constant τ (in terms of low-pass filtering RC circuits), the sampling time T_s, and the cutoff frequency f_c that is selected to implement the filter

$$\tau = \frac{1}{2\pi f_c} \rightarrow \alpha = \frac{T_s}{\tau + T_s}. \tag{15}$$

These equations are proposed to filter the absolute value of the accelerometer signal. To do this, the necessary parameters are selected in order to obtain the value of α.

Mobile device sensors can work at different sampling frequencies, but in the case at hand, $f_s = 100$ Hz is selected, which results in $T_s = 10$ ms. On the other hand, the cutoff

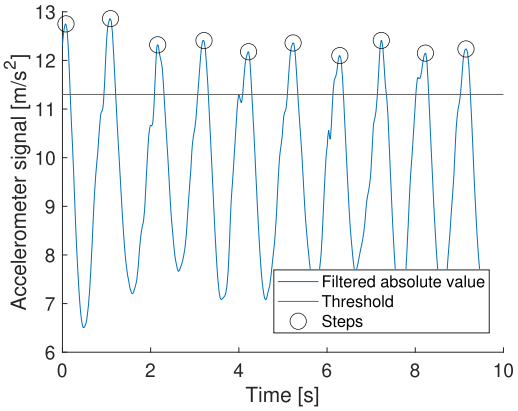

Fig. 6. Absolute value of the signal obtained from the accelerometer with low-pass filtering, step detection threshold, and steps detected.

frequency is fixed at $f_c = 15$ Hz (based on the empirical study by Wang et al. [16] and validated on this work). With these data, it is obtained that $\alpha = 0.4851$.

Once this filter has been implemented, the signal shown in Fig. 6 is obtained, where a decrease in the number of false positives is shown (detection of steps above the threshold without being a maximum).

B. Step Length

The step length is directly related to the general PDR equation (13), where $L_{k-1,k}$ represents the step length at each update of the algorithm. The subscript nomenclature $k-1, k$, therefore, refers to the distance between the occurrence of the previous event ($k-1$, previous detected step) and the current event (k, current detected step).

To determine the step length, there are several approaches that can be found in the literature. For the scenario presented on this work, it can be a constant value since there are no significant accumulative errors due to the beacons distance, or can be calculated as an average value from the error obtained between two beacons. On both situations, this value will be fixed during the position calculation of the PDR equation, so this value can be named as **L**.

C. Heading Determination

The heading determination is the parameter that is used to define the direction and trajectory followed by the user.

This parameter relies on the coordinates system of the device with respect the Earth coordinates system. The value that is used in this work is obtained directly from the device, which provides the azimuth using the rotation matrix and the inertial sensors. The usage of this heading determination is presented in the official documentation of Android devices [19].

In the PDR equation (13), this parameter is called $\psi_{k-1,k}$. It refers to the angle that the previous direction makes with respect to the current direction. Since the device is assumed to be aligned with respect to the reference system, it can be said that this angle depends only on the current direction of the user. That is, the desired steering angle satisfies $\psi_{k-1,k} = \psi_k$.

TABLE I
MOBILE DEVICE SPECIFICATIONS

Samsung Galaxy Tab S3 (SM-T820)		
Sensor	**Parameter**	**Value**
Front Camera	Model	Samsung S5K4E6XX CMOS
Front Camera	Focal Aperture	$f/2.2$
Front Camera	Focal Length	1.92 mm
Front Camera	Sensor Size	2.89×2.16 mm
Front Camera	Resolution	2560×1920 px
Front Camera	Pixel Array Size	2576×1932 px
Front Camera	Pixel Length	$1.20\,\mu$m
Inertial Sensor	Accel. + Gyro.	ST Microelectronics K6DS3TR
Inertial Sensor	Magnetometer	AKM AK09916

With all the parameters obtained, the PDR equation is rewritten as

$$\begin{cases} X_k = X_{k-1} + L \cdot \sin \psi_k \\ Y_k = Y_{k-1} + L \cdot \cos \psi_k. \end{cases} \tag{16}$$

V. RESULTS

The VLP-PDR mobile application-based IPS was specifically conceptualized for the development of a comprehensive guidance and routing application, meticulously tailored for Android devices. The experiments examining the VLP AoA-based corrections are conducted in the laboratory, whereas the rest took place at the Museo de Guadalajara, Guadalajara, Spain. The aim of this section is to demonstrate a real-world use case of indoor positioning in museums, enhancing the user's experience.

The mobile device used for the experiments is a Samsung Galaxy Tab S3 (SM-T820). It is equipped with the hardware presented in Table I. The AoA-based algorithm uses the front camera and the IMU, whereas the PDR-based algorithm uses only the IMU.

A. VLP AoA-Based Algorithm Results

The setup for these experiments involves highly precise measurements, conducted using a Leica MS60 (multistation or total station), from now on TS, and a GRZ101 tracking prism [20], assumed as the ground truth. On the other hand, the real-world measurements obtained with the mobile device and the VLP AoA-based algorithm. The TS offers a precision of ~ 2 mm over distance ranges of 1.5–10 000 m, surpassing the expected centimeter-level measurements of this work.

Fig. 7 depicts the test environment for the conducted measurements. Fig. 7(a) displays the total station used to measure the ground truth (highlighted in green) in relation to the smart light (highlighted in blue), and in Fig. 7(b), the device employed for measurements with the tracking prism is shown (highlighted in blue), securely attached.

Hence, the TS measurements serve as the ground truth. The steps for the testing scenario setup are as follows.

1) Obtain the TS coordinates in the chosen reference system, with reference to the Earth's North for (x, y, z) measurements. In this case, x is referred as easting and y as northing.
2) Measure the 3-D coordinates of the focus center in the chosen coordinate system.

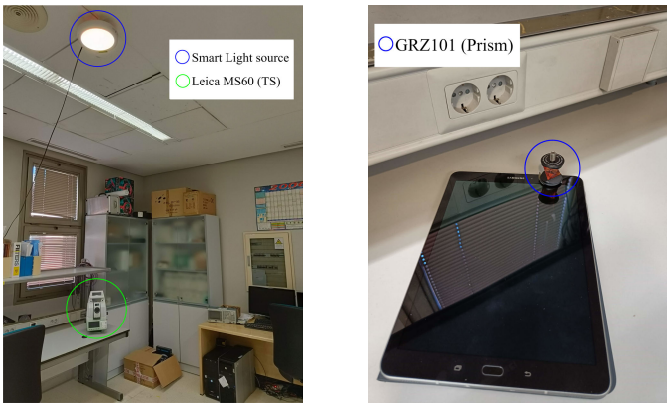

Fig. 7. Setup environment. (a) Total station and light source in the setup. (b) Mobile device with tracking prism attached.

3) Place the prism on the mobile device.
4) Measure the receiver's static position, testing the algorithm's performance under different angles, comparing results with the ground truth. This process results in 80 measurements considering users' typical hand gestures: orientation angle (azimuth) every 90° within $[-90°, 180°]$, elevation angle (pitch) every 4° within $[0°, 12°]$, and inclination angle (roll) every 4° within $[-8°, 8°]$.

The results from the static test for different positional angles are depicted in Fig. 8. The point cloud formed by blue circles represents the ground truth, measured by the TS from the tracking prism placed at the device. The point cloud formed by red crosses is the receiver's measured position, obtained by the mobile device. The black diamond represents the smart light (emitter) that is placed on a known position in the ceiling. This position is obtained with the TS, placed in $X_e = -2.35$ m and $Y_e = 1.93$ m. The TS device is placed at $(0, 0)$. Note: the mobile device is not placed under the smart light. The height of the smart light on the ceiling ($Z_e = 2.80$ m) and the mobile device ($Z_r = 1.20$ m) is known.

Significant dispersion arises from errors originating from the rotation matrix and orientation matrix acquired through the Android API, primarily influenced by the hardware specifications of the device.

The maximum error $[\max(\mathbf{E_d})]$, average error $[\mu(\mathbf{E_d})]$, variance $[\sigma^2(\mathbf{E_d})]$, and standard deviation $[\sigma(\mathbf{E_d})]$ are calculated using the Euclidean distance $(\mathbf{d})$ for the orientation, inclination, and elevation angles. The error is obtained by using each value of the point cloud with respect to its correspondence from the ground truth.

Table II presents a consolidation of such error calculations, highlighting the worst case for each experiment, based on the measurements shown in Fig. 8. Notably, the mean error obtained while changing the angles is 10.64 cm, demonstrating the precision achieved while using the VLP AoA-based algorithm. This highlights the reliability and accuracy of the approach under the experimental setup conditions.

The horizontal distance between mobile device and beacon, so-called coverage area, is measured as 1.2 m (radius) in the experimental tests. The coverage area is directly related with

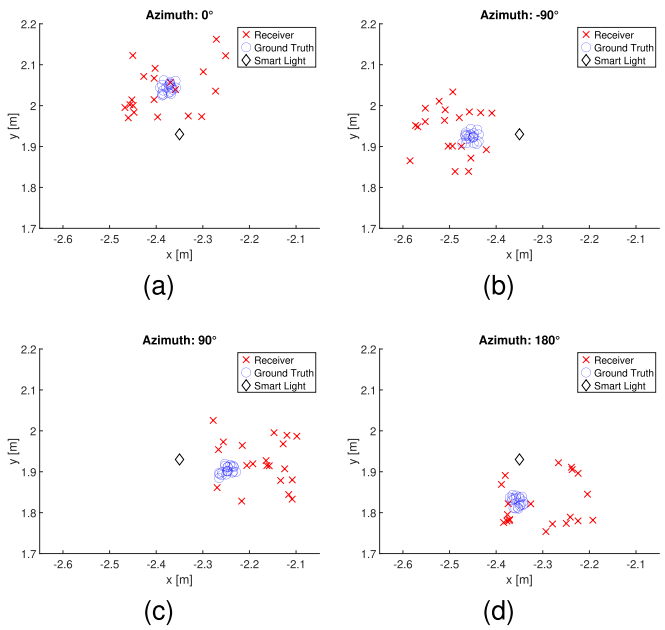

Fig. 8. VLP AoA-based algorithm on different azimuth, considering elevations, and inclinations. (a) Azimuth 0°. (b) Azimuth −90°. (c) Azimuth 90°. (d) Azimuth 180°.

TABLE II
AoA-Based Algorithm Errors Consolidation

Azimuth (°)	$\max(\mathbf{E_d})$ (m)	$\mu(\mathbf{E_d})$ (m)	$\sigma^2(\mathbf{E_d})$ (m)	$\sigma(\mathbf{E_d})$ (m)
-90	0,1389	0,0522	0,0895	0,0299
0	0,1798	0,0854	0,1625	0,0403
90	0,1727	0,1064	0,1899	0,0436
180	0,1830	0,0935	0,2567	0,0506
Pitch (°)	**$\max(\mathbf{E_d})$ (m)**	**$\mu(\mathbf{E_d})$ (m)**	**$\sigma^2(\mathbf{E_d})$ (m)**	**$\sigma(\mathbf{E_d})$ (m)**
0	0,1727	0,0801	0,1486	0,0385
4	0,1608	0,1025	0,1613	0,0402
8	0,1830	0,0953	0,2217	0,0471
12	0,1798	0,0927	0,1709	0,0413
Roll (°)	**$\max(\mathbf{E_d})$ (m)**	**$\mu(\mathbf{E_d})$ (m)**	**$\sigma^2(\mathbf{E_d})$ (m)**	**$\sigma(\mathbf{E_d})$ (m)**
-8	0,1407	0,0896	0,1388	0,0372
-4	0,1726	0,0859	0,1343	0,0366
0	0,1727	0,1020	0,1701	0,0412
4	0,1566	0,0828	0,1926	0,0439
8	0,1830	0,1030	0,2522	0,0502

the field of view of the receiver (mobile device). On the other hand, the difference in errors comes from how accurately we pinpoint the center of the focus image. Even in this difference in distances, the central point is not expected to show big changes. Also, the mistake made in figuring out the IMU angles is bigger than the one made in finding the focus image centroid. Hence, we can ignore this smaller error.

B. PDR-Based Algorithm Results

The following experiment is conducted to assess the efficacy of the PDR algorithm in the indoor environment selected.

Fig. 9 shows an example of a route obtained while using PDR algorithm. The red dots observed in Fig. 9 represent the detected steps, and the green arrow is the route provided to be followed by the user, not assumed as ground truth since it is an estimated route.

Analyzing the graphical results, while the PDR algorithm effectively provides a route within an indoor environment, it is not immune to certain limitations. The accumulated errors associated with step detection and heading determination

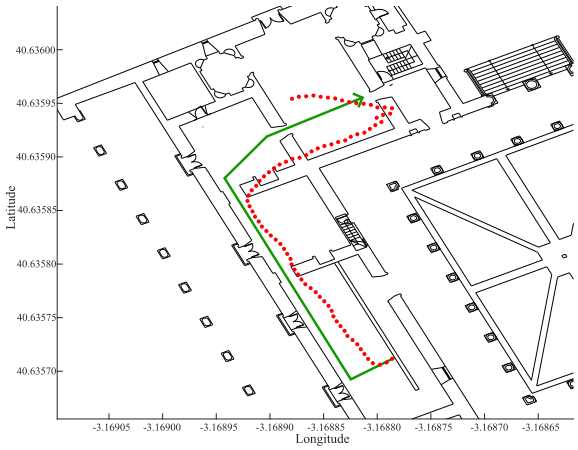

Fig. 9. PDR-based algorithm result (Route 1).

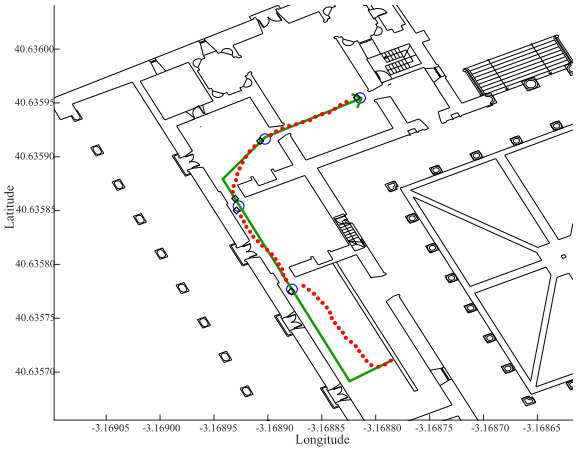

Fig. 10. Integration of the AoA and PDR algorithms (Route 1).

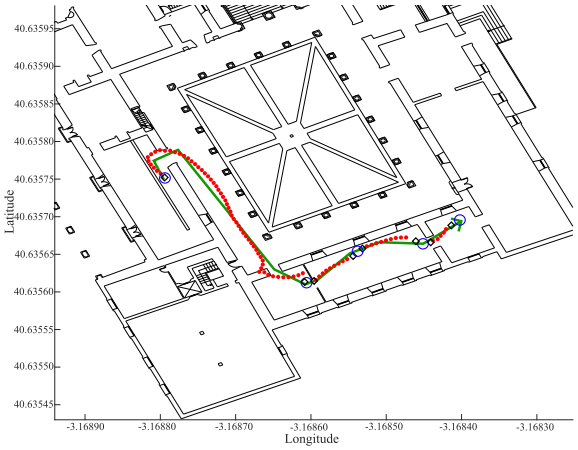

Fig. 11. Integration of the AoA and PDR algorithms (Route 2).

lead to slight deviations from the expected route, particularly noticeable during user turns. These deviations, although present, do not exceed 3 m, which is an acceptable range for leisure indoor navigation purposes, such as the museum use case.

Additionally, it is essential to note that the performance of the PDR algorithm is influenced by environmental factors within the indoor setting. The presence of metals in the environment poses a particular challenge, as the IMU relies on the magnetometer for orientation calculations. Consequently, the interference caused by metallic elements can lead to inaccuracies in the determination of the user's orientation, thereby impacting the overall reliability of the PDR system. Understanding the impact of environmental variables on the algorithm's functionality is critical for devising effective strategies to mitigate potential errors and enhance the algorithm's robustness in diverse indoor environments. This is the case to perform an integration with the VLP solution.

C. VLP-PDR Integration Results

The experiments in this section aim to demonstrate the efficacy of integrating both algorithms into a unified solution. The implementation of the AoA-correction algorithm reduces errors resulting from device inclinations. Additionally, the integration of this solution with the PDR algorithm effectively mitigates cumulative errors associated with the environment, particularly during navigation around smart lights.

Fig. 10 illustrates the integration of both algorithms. The red dots represent the detected PDR steps, while the black diamonds denote the AoA detections. The blue circles indicate the locations of the strategically positioned light sources on the ceiling. The green arrow represents the route to be followed by the user. The data source is the same as that obtained in Section V-B, but calculated with the smart lights powered on. Notably, the distinct alignment of the AoA detection attests to the precision of the algorithm in recalibrating the user's position relative to the physical location of the light sources, resulting in minor deviations in the positioning route.

Comparatively, when examining the results in Fig. 9, the integrated methodology demonstrates a more organic and accurate route, particularly notable in contrast to the cumulative error. By updating the position using the VLP solution, the cumulative error associated with the PDR algorithm is alleviated.

A secondary instance of this approach is depicted in Fig. 11, employing the same color coding as the preceding illustration. Under these circumstances, it becomes apparent that the cumulative error generated by the PDR algorithm increases with greater distances between two light sources, as indicated between beacons 1 and 2. Consequently, the recommended approach for deployment involves striking a balance between the costs associated with the number of beacons and the requisite precision for the solution.

In conclusion, Figs.10 and 11 show that the accumulated errors from the PDR algorithm are reset during the moments when the VLP AoA-based algorithm is employed. Specifically, the mean errors concerning the path to follow (in green) are on the order of 0.85 m, providing a performance that is valid for the museum's context. Finally, a comparative table is provided, contrasting similar works from the state-of-the-art and our results. Table III presents comparative results for: 1) VLP algorithms; 2) PDR algorithms; and 3) integrated algorithms.

D. User Interface

To facilitate visitor navigation and contextual information retrieval within the museum, an intuitive user interface

TABLE III
STATE-OF-THE-ART COMPARISON

Technology	Work	$\mu(\mathbf{E_d})$ (m)
VLP	[21]	0.33
VLP	[22]	0.13
VLP	[23]	0.20
VLP	Ours	0.10
PDR	[16]	2.00
PDR	[24]	2.00
PDR	[25]	1.95
PDR	Ours	3.00
VLP-PDR	[26]	1.00
UWB-PDR	[27]	2.00
WIFI-PDR-EKF	[28]	1.4
VLP-PDR	Ours	0.85

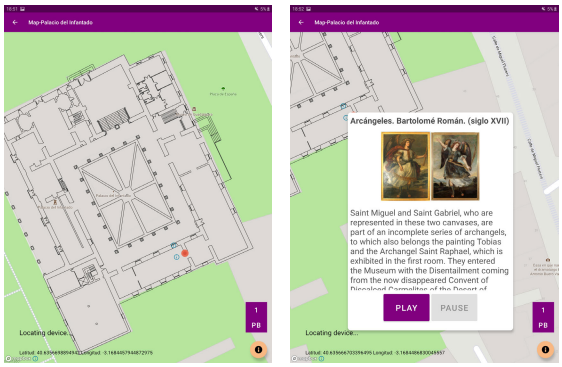

(a) (b)

Fig. 12. (a) Interactive map and (b) POI information.

integrates with the mobile application. The accompanying database stores exhibition details, images, and historical information in English and Spanish. A user-friendly interface is vital for enhancing visitor satisfaction, emphasizing usability, accessibility, and visual appeal. Clear design and direct database downloading during the initial setup optimize the user's experience, enabling intuitive navigation without the need for continuous Internet connectivity.

Fig. 12(a) illustrates the appearance of the interactive map as seen by the user. Here, the current position of the visitor is presented as a red circle, along with the nearby POIs represented by blue information icons. These POIs are displayed based on proximity, meaning that they are obtained as the user approaches these elements. This functionality is designed to allow users to navigate freely through the museum. Fig. 12(b) shows the relevant information obtained from the POI while pressing on it. The information contains additional descriptions from the ones provided within the museum as well as an audio-guide fragment. Both information sources are shared in English or Spanish, depending on the smartphone's language.

Fig. 13(a) and (b) depicts real-world scenarios within the museum, demonstrating the practical usage of the application. Users are shown interacting with museum exhibits, holding their devices in front of a piece. The mobile screen showcases the information obtained through the POIs that appear nearby the user's position. As shown, it matches with the pieces.

Finally, here is an accompanying video that illustrates the experimental setup and results discussed in this article. The video can be accessed at: https://youtu.be/4Co6H1KluV4.

(a) (b)

Fig. 13. (a) and (b) Real-world scenario within the museum exhibition.

VI. CONCLUSION

The research outcomes reveal significant insights into the performance and applicability of the VLP-PDR mobile application-based IPS in a real-world scenario, particularly within the context of a museum environment. The experiments conducted demonstrate the capabilities and limitations of the VLP AoA-based algorithm, the PDR-based algorithm, and the integration of these two techniques, as well as the effectiveness of the designed user interface.

The VLP AoA-based algorithm consistently demonstrated precision within 10 cm, as evidenced by the experiments conducted in both controlled laboratory settings and the actual museum environment.

Similarly, the PDR-based algorithm showcased its efficacy in providing reliable indoor positioning guidance, with minor deviations from the expected route, showcasing mean errors of 3 m, predominantly influenced by environmental factors such as the presence of metallic elements.

The integration of the VLP AoA-based algorithm with the PDR algorithm exhibited a significant enhancement in the system's accuracy and reliability. The recalibration of the user's position in relation to the physical locations of the smart lights effectively mitigated cumulative errors, resulting in a more natural and precise route for the users with a mean error of 0.85 m in the experiments conducted.

Furthermore, the intuitive user interface design contributed to the overall user experience, allowing visitors to navigate the museum effortlessly and access contextual information about different exhibitions.

Future research directions involve integrating advanced machine learning techniques for enhanced accuracy, incorporating augmented reality elements for increased user immersion, and implementing gamification and personalized recommendation systems for improved user engagement. Enhancements to the PDR component include dynamic step detection thresholds, adjustable step lengths, and dynamic user orientation updates, based on Kalman or particle filtering principle. Additionally, integrating a mechanism to detect the device's held height could further enhance the precision of the positioning system based on the AoA-based algorithm, optimizing its performance within museum settings.

ACKNOWLEDGMENT

Álvaro De-La-Llana-Calvo, José Luis Lázaro-Galilea, and Antoni Pérez-Navarro: conceptualization; Aitor Alcázar-Fernández, Álvaro De-La-Llana-Calvo, and Rubén Gil-Vera: data curation and software; Álvaro De-La-Llana-Calvo, José Luis Lázaro-Galilea, Alfredo Gardel-Vicente, and Aitor Alcázar-Fernández: formal analysis and validation; Alfredo Gardel-Vicente, José Luis Lázaro-Galilea, and Álvaro De-La-Llana-Calvo: funding acquisition and project administration; Aitor Alcázar-Fernández, Álvaro De-La-Llana-Calvo, José Luis Lázaro-Galilea, Alfredo Gardel-Vicente, Antoni Pérez-Navarro, and Rubén Gil-Vera: investigation and writing—review and editing; José Luis Lázaro-Galilea and Álvaro De-La-Llana-Calvo: methodology and resources; José Luis Lázaro-Galilea and Antoni Pérez-Navarro: supervision; and Álvaro De-La-Llana-Calvo, José Luis Lázaro-Galilea, and Aitor Alcázar-Fernández: visualization and writing—original draft. All authors read and agreed to the published version of this article. The authors would like to express their gratitude for the collaboration of the Museo de Guadalajara, Guadalajara, Spain.

REFERENCES

[1] I. N. de Estadística, "Equipamiento y uso de tic en los hogares–año 2022," Instituto Nacional de Estadística, Spain, Tech. Rep. TIC_H-2022, Jun. 2022.

[2] A. Damala, I. Ruthven, and E. Hornecker, "The MUSETECH model," *J. Comput. Cultural Heritage*, vol. 12, no. 1, pp. 1–22, Feb. 2019.

[3] J. M. F. Rodrigues, C. M. Q. Ramos, J. A. R. Pereira, J. D. P. Sardo, and P. J. S. Cardoso, "Mobile five senses augmented reality system: Technology acceptance study," *IEEE Access*, vol. 7, pp. 163022–163033, 2019.

[4] H. Koyuncu and S. H. Yang, "A survey of indoor positioning and object locating systems," *Int. J. Comput. Sci. Netw. Secur.*, vol. 10, no. 5, pp. 121–128, 2010.

[5] R. Mautz, "Indoor positioning technologies," Ph.D. thesis, Dept. Civil, Environ. Geomatic Eng., Inst. Geodesy Photogramm., ETH Zürich, Zürich, Switzerland, 2012.

[6] A. Yassin et al., "Recent advances in indoor localization: A survey on theoretical approaches and applications," *IEEE Commun. Surveys Tuts.*, vol. 19, no. 2, pp. 1327–1346, 2nd Quart., 2017.

[7] X. Guo, N. Ansari, F. Hu, Y. Shao, N. R. Elikplim, and L. Li, "A survey on fusion-based indoor positioning," *IEEE Commun. Surveys Tuts.*, vol. 22, no. 1, pp. 566–594, 1st Quart., 2020.

[8] E. Aparicio-Esteve, Á. Hernández, J. Ure na, J. M. Villadangos, and F. Ciudad, "Estimation of the polar angle in a 3D infrared indoor positioning system based on a QADA receiver," in *Proc. Int. Conf. Indoor Positioning Indoor Navigat. (IPIN)*, Sep. 2019, pp. 1–8.

[9] T. Arai, T. Yoshizawa, T. Aoki, K. Zempo, and Y. Okada, "Evaluation of indoor positioning system based on attachable infrared beacons in metal shelf environment," in *Proc. IEEE Int. Conf. Consum. Electron. (ICCE)*, Jan. 2019, pp. 1–4.

[10] K. Mannay, J. Ureña, Á. Hernández, J. M. Villadangos, M. Machhout, and T. Aguili, "Evaluation of multi-sensor fusion methods for ultrasonic indoor positioning," *Appl. Sci.*, vol. 11, no. 15, p. 6805, Jul. 2021.

[11] D. Gualda et al., "LOCATE-U.S.: Indoor positioning for mobile devices using encoded ultrasonic signals, inertial sensors and graph-matching," *Sensors*, vol. 21, no. 6, p. 1950, Mar. 2021.

[12] Y. Zhuang et al., "A survey of positioning systems using visible LED lights," *IEEE Commun. Surveys Tuts.*, vol. 20, no. 3, pp. 1963–1988, 3rd Quart., 2018.

[13] Á. De-La-Llana-Calvo, J. L. Lázaro-Galilea, A. Alcázar-Fernández, A. Gardel-Vicente, I. Bravo-Muñoz, and A. Iamnitchi, "Accuracy and precision of agents orientation in an indoor positioning system using multiple infrastructure lighting spotlights and a PSD sensor," *Sensors*, vol. 22, no. 8, p. 2882, Apr. 2022.

[14] A. R. Jimenez, F. Seco, C. Prieto, and J. Guevara, "A comparison of pedestrian dead-reckoning algorithms using a low-cost MEMS IMU," in *Proc. IEEE Int. Symp. Intell. Signal Process.*, Aug. 2009, pp. 37–42.

[15] H. Guo and M. Uradzinski, "The usability of MTI IMU sensor data in PDR indoor positioning," in *Proc. 25th Saint Petersburg Int. Conf. Integr. Navigat. Syst. (ICINS)*, May 2018, pp. 1–4.

[16] B. Wang, X. Liu, B. Yu, R. Jia, and X. Gan, "Pedestrian dead reckoning based on motion mode recognition using a smartphone," *Sensors*, vol. 18, no. 6, p. 1811, Jun. 2018.

[17] Y.-S. Li and F.-S. Ning, "Low-cost indoor positioning application based on map assistance and mobile phone sensors," *Sensors*, vol. 18, no. 12, p. 4285, Dec. 2018.

[18] J. Racko, P. Brida, A. Perttula, J. Parviainen, and J. Collin, "Pedestrian dead reckoning with particle filter for handheld smartphone," in *Proc. Int. Conf. Indoor Positioning Indoor Navigat. (IPIN)*, Oct. 2016, pp. 1–7.

[19] *Android Developers: Descripción General de Sensores*, Android, Mountain View, CA, USA, 2019.

[20] *Leica Nova Ms60 Datasheet*, Leica, Wetzlar, Germany, 2020.

[21] J. Fang et al., "High-speed indoor navigation system based on visible light and mobile phone," *IEEE Photon. J.*, vol. 9, no. 2, pp. 1–11, Apr. 2017.

[22] R. Zhang, W.-D. Zhong, Q. Kemao, and S. Zhang, "A single LED positioning system based on circle projection," *IEEE Photon. J.*, vol. 9, no. 4, pp. 1–9, Aug. 2017.

[23] Z. Wang, Z. Yang, Q. Huang, L. Yang, and Q. Zhang, "ALS-P: Light weight visible light positioning via ambient light sensor," in *Proc. IEEE Conf. Comput. Commun. (INFOCOM)*, Apr. 2019, pp. 1306–1314.

[24] W. Kang and Y. Han, "SmartPDR: Smartphone-based pedestrian dead reckoning for indoor localization," *IEEE Sensors J.*, vol. 15, no. 5, pp. 2906–2916, May 2015.

[25] J.-S. Lee and S.-M. Huang, "An experimental heuristic approach to multi-pose pedestrian dead reckoning without using magnetometers for indoor localization," *IEEE Sensors J.*, vol. 19, no. 20, pp. 9532–9542, Oct. 2019.

[26] Y. Wang and H. Zhao, "Improved smartphone-based indoor pedestrian dead reckoning assisted by visible light positioning," *IEEE Sensors J.*, vol. 19, no. 8, pp. 2902–2908, Apr. 2019.

[27] F. Zampella, R. A. R. Jiménez, and F. Seco, "Robust indoor positioning fusing PDR and RF technologies: The RFID and UWB case," in *Proc. Int. Conf. Indoor Positioning Indoor Navigat.*, Oct. 2013, pp. 1–10.

[28] J. Sun, X. Yu, D. Liu, Y. Zhai, and C. Wang, "Research on indoor location technology based on the fusion of WiFi and PDR," in *Proc. 13th Int. Conf. Intell. Comput. Technol. Autom. (ICICTA)*, Oct. 2020, pp. 416–419.

Aitor Alcázar-Fernández received the B.Sc. degree in telecommunications engineering from the Technical University of Madrid, Madrid, Spain, in 2019, and the M.Sc. degree in telecommunications engineering from the Open University of Catalonia, Barcelona, Spain, in 2022. He is currently pursuing the Ph.D. degree in electronics with the University of Alcalá, Alcalá de Henares, Spain.

He is a Madrid-Based Researcher with BDS Research and Development Spain (Eviden), Madrid. He leads European projects and participates in conferences and congresses. His research interests include indoor positioning based on visible light, the Internet of Things, and smart cities.

Álvaro De-La-Llana-Calvo received the Ph.D. degree in electronics from the University of Alcalá, Alcalá de Henares, Spain, in 2020.

He currently holds the position of Lecturer at the Department of Electronics, University of Alcalá. His research interests include indoor positioning by infrared and visible light, range sensor fusion, and smart devices.

José Luis Lázaro-Galilea (Member, IEEE) received the Ph.D. degree in telecommunication engineering from the University of Alcalá, Alcalá de Henares, Spain, in 1998.

He currently holds the position of Full Professor at the Department of Electronics, University of Alcalá. His research interests include indoor positioning by infrared and visible light, range sensor fusion, and smart devices.

Antoni Pérez-Navarro (Member, IEEE) received the B.S. and Ph.D. degrees in physics from the Universitat Autònoma de Barcelona (UAB), Barcelona, Spain, in 1995 and 2000, respectively.

He has been an Aggregate Professor with the Faculty of Computer Science, Multimedia and Telecommunication, Universitat Oberta de Catalunya (UOC), Barcelona, since 2005. His main research interests include indoor positioning, prevention of diseases via technology, and e-learning of sciences.

Dr. Pérez-Navarro is member of the Steering Committee of IPIN.

Rubén Gil-Vera received the B.Sc. degree in electronics engineering from the University of Alcalá, Alcalá de Henares, Spain, in 2022, where he is pursuing the M.Sc. degree.

He is currently working as a Research Assistant with the Department of Electronics, University of Alcalá. His research interests include indoor positioning by visible light and smart devices.

Alfredo Gardel-Vicente born in Guadalajara, Spain. He received the Ph.D. degree in telecommunications engineering and computer vision from the University of Alcalá, Alcalá de Henares, Spain, and the University of Clermont-Ferrand, Clermont-Ferrand, France, in 2004.

He currently holds the position of Full Professor at the Department of Electronics, University of Alcalá. Prof. Gardel-Vicente's primary research interests include programmable hardware/software embedded systems, computer vision, and smart devices.